UniAct: Unified Motion Generation and Action Streaming for Humanoid Robots

Nan Jiang[1,2,3,9,11*] Zimo He[4,2,9,11*] Wanhe Yu[1,3,5,9,11] Lexi Pang[1,3,5,9,11]

Yunhao Li[6,3,9,11] Hongjie Li[7,3,9,11] Jieming Cui[1,2,3,9,11] Yuhan Li[8,2]

Yizhou Wang[4,9,10] Yixin Zhu[3,1,9,11,12 ✉] Siyuan Huang[2,9 ✉]

[1] Institute for AI, Peking University [2] Beijing Institute for General Artificial Intelligence (BIGAI)

[3] School of Psychological and Cognitive Sciences, Peking University [4] School of Computer Science, Peking University

[5] Yuanpei College, Peking University [6] School of Foreign Languages, Peking University [7] School of EECS, Peking University

[8] Huazhong University of Science and Technology [9] State Key Lab of General AI [10] Nat'l Eng. Research Center of Visual Technology

[11] Beijing Key Laboratory of Behavior and Mental Health, Peking University

[12] Embodied Intelligence Lab, PKU-Wuhan Institute for Artificial Intelligence

[*] Equal contribution ✉ yixin.zhu@pku.edu.cn, syhuang@bigai.ai

https://jnnan.github.io/uniact/

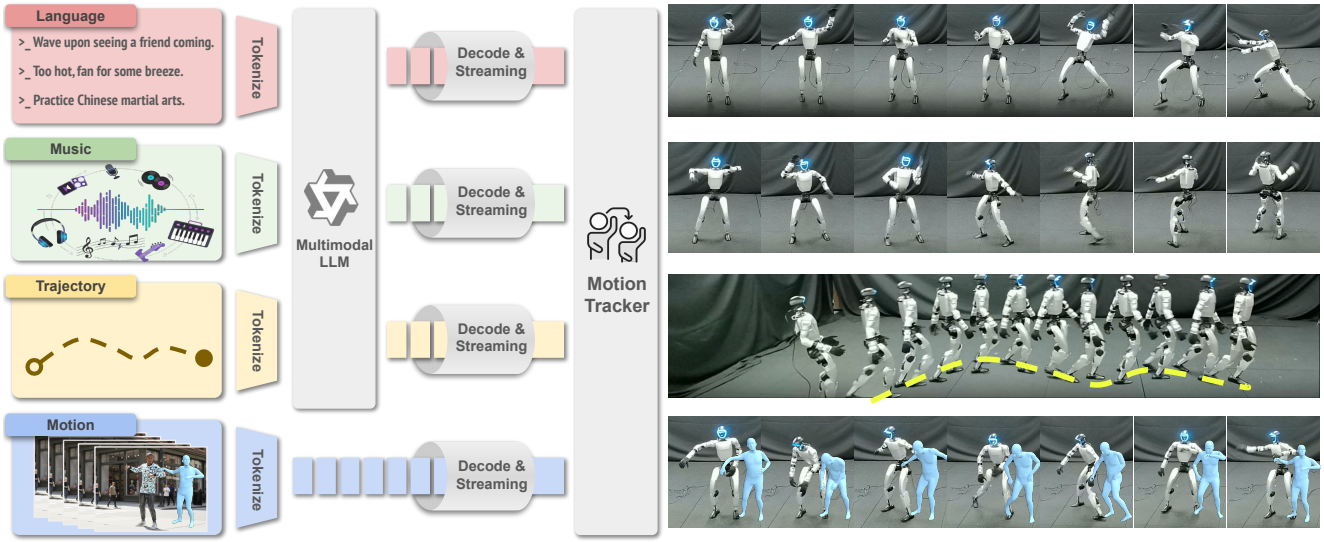

(a) Multimodal motion generation (b) Motion decoding and streaming (c) Robot execution

Figure 1. **UniAct, a unified framework for multimodal motion generation and action streaming.** UniAct enables humanoid robots to interpret and execute diverse multimodal instructions—including natural language, musical rhythms, spatial trajectories, and reference motions—with high-fidelity performance. The architecture consists of three core components: (a) a fine-tuned MLLM that translates heterogeneous inputs into discrete motion tokens via a shared codebook using FSQ; (b) a causal decoding and streaming pipeline that ensures low-latency delivery of reference motions; and (c) a robust motion tracker that executes the generated motions while maintaining dynamic balance.

Abstract

A long-standing objective in humanoid robotics is the realization of versatile agents capable of following diverse multimodal instructions with human-level flexibility. Despite advances in humanoid control, bridging high-level multimodal perception with whole-body execution remains a significant bottleneck. Existing methods often struggle to translate heterogeneous instructions—such as language, music, and trajectories—into stable, real-time actions. Here we show that UniAct, a two-stage framework integrating a fine-tuned Multimodal Large Language Model (MLLM) with a causal streaming pipeline, enables humanoid robots to execute multimodal instructions with sub-500 ms latency. By unifying inputs through a shared discrete codebook via Finite Scalar Quantization (FSQ), UniAct ensures cross-modal alignment while constraining motions to a physically grounded manifold. This approach yields a 19% improvement in the success rate of zero-shot tracking of im-

perfect reference motions. We validate UniAct on UA-Net, our 20-hour humanoid motion benchmark, demonstrating robust generalization across diverse real-world scenarios. Our results mark a critical step toward responsive, general-purpose humanoid assistants capable of seamless interaction through unified perception and control.

1. Introduction

Advances in humanoid control have yielded remarkable progress in low-level tracking [36, 77], force control [85], and agile locomotion [39, 63]. These developments enable robots to execute complex physical tasks with unprecedented precision. However, a fundamental gap persists between high-level perception and low-level execution, limiting humanoid systems' ability to translate multimodal instructions into coherent, stable actions seamlessly.

Existing attempts to bridge this perception-control gap generally follow two bifurcated paradigms: one-step end-to-end mapping or two-step hierarchical pipelines. One-step methods [60, 75], often utilizing variational autoencoders (VAEs) or diffusion models, offer low latency but typically struggle with the long-term temporal dependencies and cross-modal reasoning required for complex instructions. Conversely, two-step methods [20, 45] decouple motion generation from execution; while this improves instruction comprehension, it introduces significant computational overhead and real-time planning challenges. Furthermore, both paradigms remain brittle when encountering out-of-distribution (OOD) observations or imperfect human demonstrations, often generating physically infeasible motions that result in hardware instability or falls.

The emergence of MLLMs [42, 84, 86] and robust motion trackers [20, 36] provides a promising pathway to resolve this tension. MLLMs excel at reasoning across diverse modalities, while modern trackers can execute reference motions with high fidelity. Leveraging these breakthroughs, we introduce UniAct, a unified framework that harmonizes high-level multimodal perception with low-level whole-body control via a decoupled two-stage architecture.

In the first stage, a fine-tuned MLLM processes diverse inputs—including language, music, and trajectories—to generate discrete motion tokens via a unified codebook. These tokens are then streamed to the second stage, where a causal decoder translates them into real-time commands for a robust motion tracker. This design introduces three key innovations: (i) a unified token representation that facilitates seamless cross-modal translation, (ii) a next-token prediction paradigm that minimizes response latency, and (iii) a discrete action space that restricts generation to a physically grounded manifold, inherently improving tracking robustness against OOD inputs.

Our evaluation demonstrates UniAct's versatility across a spectrum of tasks. The system accurately interprets complex sequential commands, synchronizes expressive dance movements with real-time musical beats, and follows precise spatial trajectories while maintaining natural gaits. Notably, our framework achieves a 19% improvement in zero-shot tracking of low-quality reference motions compared to state-of-the-art (SOTA) baselines. These capabilities were validated through more than 1,000 simulation trials and 100+ hours of real-world operation on physical humanoid platforms.

To advance reproducible research on humanoid control, we contribute UA-Net, a comprehensive 20-hour dataset of high-quality robot motions. Meticulously organized in lexicographic order and annotated in multiple modalities, including linguistic descriptions and rhythmic patterns, UA-Net serves as a rigorous benchmark for evaluating the multimodal instruction following capabilities.

In summary, our key contributions are:

- We present UniAct, a unified framework that integrates MLLMs with robust whole-body tracking, achieving a response latency of sub-500 ms for multimodal humanoid control.
- We introduce a unified motion embedding method that leverages shared discrete tokens to enable seamless cross-modal translation and enhanced tracking stability.
- We demonstrate the robust generalization of UniAct through extensive real-world experiments across diverse linguistic, rhythmic, and trajectory following tasks.
- We establish UA-Net, a large-scale multimodal benchmark and standardized evaluation protocol to facilitate future research on humanoid embodied intelligence.

2. Related work

Whole-body humanoid control Humanoid control has its foundations in physics-based animation, where reinforcement learning is extensively used to track reference motions with high fidelity [43, 49, 50, 59]. To facilitate high-level task specification, research has introduced adversarial embeddings [11, 51] and task-specific latent policies [47, 64] to enable behavioral synthesis through compositional inputs [8, 68, 72, 74]. Recent approaches further integrate diffusion-based motion planning with robust tracking policies for multi-task character control [67]. Despite their effectiveness in simulation, these animation-centric methods fundamentally rely on privileged observations that are typically unavailable in real-world settings.

In the physical domain, humanoid control has progressed through robust low-level mechanisms [17, 20, 22, 23, 25, 29, 36, 77, 80, 81] capable of handling diverse modalities, including directional locomotion [6, 14, 56, 57, 63], end-effector pose specification [20, 32], and natural language commands [34, 60, 75]. However, existing frameworks generally treat these modalities in isolation through distinct

injection mechanisms [12, 75]. Language-conditioned approaches, in particular, face a stark trade-off: hierarchical pipelines [20, 21] often sacrifice real-time responsiveness for comprehension, while end-to-end architectures that incorporate language latents directly [34, 60] often struggle with complex semantic reasoning. Consequently, the field lacks a unified framework capable of processing heterogeneous multimodal inputs while maintaining deterministic, real-time control.

Multimodal human motion generation Motion generation has evolved from specialized text-driven approaches [1, 2, 9, 15, 18, 24, 37, 38, 41, 52, 53, 55, 65, 66, 82, 83] to versatile systems incorporating diverse control modalities, such as spatial trajectories [26, 40, 54, 73] and rhythmic musical signals [3, 27, 31, 62, 69, 70]. Recent unified frameworks [5, 33, 35, 42, 84, 86] seek to harmonize these modalities within a single architecture: M^{3}GPT [42] employs discrete vector quantization for cross-modal synthesis, UDE [86] utilizes modality-agnostic transformers, and MotionCraft [5] adopts a coarse-to-fine training strategy for varying control granularities. While these methods achieve impressive offline generation quality, they predominantly rely on iterative diffusion processes or multi-stage pipelines that introduce substantial computational latency. Consequently, they remain ill-suited for humanoid control applications that demand instantaneous, real-time response.

Humanoid motion dataset Progress in humanoids is significantly hampered by the scarcity of high-quality datasets compared to fixed-base manipulation platforms [7, 13, 16, 71]. To bridge this gap, motion retargeting techniques [43, 78, 79] have been developed to adapt human MoCap data from general-purpose repositories [19, 28, 44] to humanoid morphologies. Specialized datasets like OmniH2O [20], OmniRetarget [76], and TWIST [80] have further advanced the field by providing loco-manipulation data tailored to specific robot embodiments. However, existing datasets focus on physical trajectories while neglecting the underlying semantic meanings and the need for multimodal alignment. This lack of comprehensive, semantically rich benchmarks constrains the development of humanoids capable of following multifaceted, complex instructions.

3. The UniAct model

UniAct addresses the challenge of translating diverse multimodal instructions into robust humanoid motion through a unified three-stage pipeline, as illustrated in Fig. 1. The framework consists of: (i) FSQ-based instruction tokenization that unifies heterogeneous inputs [46], (ii) MLLM-driven motion generation that produces temporally coherent motion sequences, and (iii) real-time whole-body tracking that executes generated motions on physical hardware.

As detailed in Fig. 2, the system first encodes text, music, trajectories, and reference motions into a shared discrete

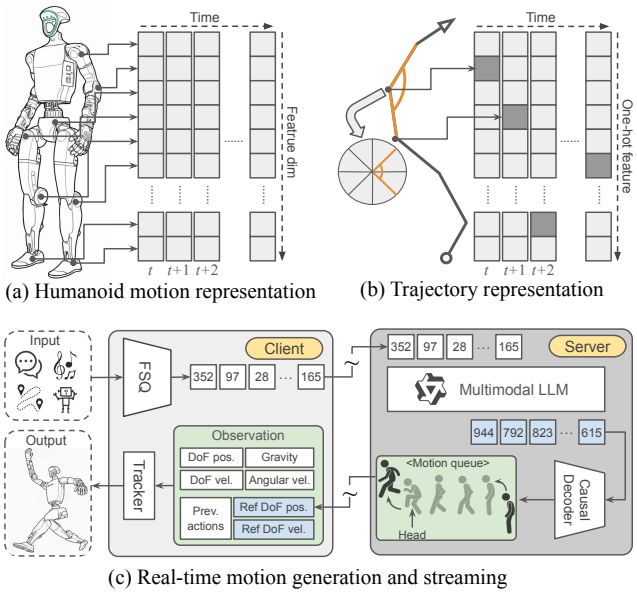

Figure 2. **Overview of UniAct and multimodal representations.** (a) Humanoid motion is represented as temporal sequences of DoF positions, tokenized via FSQ. (b) Trajectory features are one-hot encoded based on the turning angle degree of segmented paths. (c) System architecture: the server-side MLLM processes multimodal inputs (text, music, trajectory) and FSQ-tokenized motions to autoregressively generate motion tokens; a causal decoder transforms tokens to continuous DoF positions, which are streamed to the client and executed by the tracking controller for real-time motion synthesis.

token representation. A fine-tuned MLLM then processes these tokens to autoregressively generate motion sequences. Finally, a causal decoder streams the generated tokens to a robust motion tracker, enabling immediate execution on the humanoid platform with sub-500 ms latency.

3.1. Problem formulation

We formulate the multimodal humanoid control problem as follows. Given a multimodal instruction $\mathcal{C} = \{\mathcal{C}_{\text{text}}, \mathcal{C}_{\text{music}}, \mathcal{C}_{\text{traj}}, \mathcal{C}_{\text{motion}}\}$, where each component represents an optional control signal, UniAct generates a temporal sequence of target degree of freedom (DoF) positions $\mathbf{p}_t \in \mathbb{R}^D$ at each control timestep t, with D denoting the robot's total DoF. The key challenge lies in bridging the semantic gap between high-level multimodal instructions and low-level joint-space commands while maintaining real-time performance and physical feasibility.

3.2. Multimodal instruction tokenization

To enable unified processing across heterogeneous modalities, we map continuous input signals $\mathbf{X}$ into a discrete latent space compatible with autoregressive language modeling. Our tokenization strategy adapts to the distinct physical and semantic characteristics of each modality while maintaining a shared discrete vocabulary.

Text Text instructions are tokenized using the native vocabulary of Qwen2.5 [4], directly leveraging the model's pre-trained word embeddings and linguistic understanding capabilities. Unlike other modalities described below, text requires no additional encoding.

Music Music signals are processed at 30 Hz following the AIST++ [30] protocol to extract temporal features. At each timestep, we compute a 35-dimensional feature vector comprising: the envelope (capturing amplitude variations), 20 MFCC coefficients (representing timbral characteristics), 12 chroma features (encoding harmonic content), and binary indicators for beat peaks and onsets. This representation captures both rhythmic structure and timbral qualities essential for dance generation.

Trajectory Trajectories are represented as the angles of line segments (Fig. 2(b)). We focus on heading direction variations to capture locomotion patterns while maintaining computational efficiency. The continuous trajectory is segmented at 5 FPS; at each frame i, we compute the root displacement in the previous frame's coordinate system:

$$\mathbf{r}_i = \mathbf{R}_{i-1}^{\mathrm{T}}(\mathbf{p}_i - \mathbf{p}_{i-1}) \in \mathbb{R}^3, \tag{1}$$

where $\mathbf{p}_i$ denotes the root position and $\mathbf{R}_{i-1}$ is the rotation matrix at frame $i-1$. This formulation ensures orientation-invariant encoding. The angular difference in heading direction is then discretized into 6-degree bins, yielding a compact codebook of size $360/6 = 60$.

Motion Reference motions are represented directly as humanoid DoF positions, eliminating the need for retargeting and enabling end-to-end control. For the Unitree-G1 robot with 29 DoFs, each frame is encoded as $\mathbf{q}_i \in \mathbb{R}^{29}$ containing all joint angle values.

To unify music, trajectory, and motion representations into discrete tokens compatible with autoregressive language modeling, we employ FSQ. For music and motion modalities, we train separate encoder-decoder pairs that compress continuous features into latent representations, which are then element-wise quantized:

$$\mathrm{FSQ}(\mathbf{z}) = \mathrm{round}(\tanh(\mathbf{z}) \cdot \mathbf{L}), \tag{2}$$

where $\mathbf{z}$ denotes the encoder output and $\mathbf{L}$ specifies the quantization levels per dimension. Both encoder and decoder are implemented as 1D convolutional networks with residual connections, trained to minimize reconstruction loss $\mathcal{L}_{\mathrm{FSQ}} = ||\mathbf{X} - \hat{\mathbf{X}}||_2^2$ (details in Sec. B.1). This architecture preserves temporal coherence while maintaining computational efficiency. The quantized latents are subsequently mapped to discrete token indices, creating modality-specific vocabularies $\mathcal{V}_{\mathrm{music}}$, $\mathcal{V}_{\mathrm{traj}}$, and $\mathcal{V}_{\mathrm{motion}}$.

3.3. Motion generation

We fine-tune Qwen2.5-3B [4] to autoregressively predict motion tokens conditioned on multimodal inputs. Our approach unifies all modalities through early fusion, constructing a shared vocabulary by concatenating tokens:

$$\mathcal{V}_{\mathrm{unified}} = \mathcal{V}_{\mathrm{text}} \cup \mathcal{V}_{\mathrm{music}} \cup \mathcal{V}_{\mathrm{traj}} \cup \mathcal{V}_{\mathrm{motion}}. \tag{3}$$

To maintain a manageable vocabulary size, we substitute the least frequent text tokens with tokens from other modalities. This substitution preserves the model's capacity for common linguistic instructions while accommodating the additional modality-specific vocabularies.

Sequence structure and training During training, we wrap each modality's token sequence with special delimiter tokens that clearly delineate modality boundaries. The complete input sequence takes the form of a concatenation of all available modalities—each enclosed by its respective delimiters—followed by the target motion sequence. This explicit boundary marking allows the model to distinguish between different conditioning modalities and the motion tokens to be predicted.

To support generation with arbitrary-length conditions, we apply a sliding window approach to trajectory and music modalities during training. Specifically, we randomly sample fixed-length segments from the full token sequences of these modalities. This approach enables the model to learn from diverse temporal contexts while maintaining computational efficiency through bounded sequence lengths.

The model is optimized via standard autoregressive language modeling:

$$\mathcal{L}_{\mathrm{gen}} = -\sum_{t=1}^{T} \log P(\mathbf{s}_t^{\mathrm{motion}} | \mathbf{s}_{<t}, \mathcal{C}), \tag{4}$$

where $\mathbf{s}_{<t}$ represents all preceding tokens (including both conditioning modalities and previously generated motion tokens), and $\mathcal{C}$ denotes the multimodal instruction context.

Inference During inference, the model autoregressively generates motion tokens conditioned on the input modalities. The generated discrete tokens are then decoded back to continuous DoF positions through the trained FSQ decoder, producing target reference motions for the humanoid tracking controller.

3.4. Causal motion decoding

To enable real-time motion execution, we implement a causal decoding mechanism that transforms generated motion tokens into humanoid DoF positions in a streaming fashion. The causal constraint ensures that the decoded motion at timestep t depends only on tokens up to time t, enabling online inference without future information:

$$\mathbf{h}_t = \sum_{k=0}^{K-1} \mathbf{W}_k \cdot \mathbf{h}_{t-k} + \mathbf{b}, \tag{5}$$

where K denotes the kernel size, and $\mathbf{W}_k$ and $\mathbf{b}$ are learned convolution parameters. To balance computational

Id	Verb	Description
1	**A**ccuse	The teacher accused the student of copying a classmate's homework.
2	**A**pproach	She gently approached her, seeking comfort and support.
3	**A**ssist	He assists the blind in crossing the road.
4	**A**void	He avoided it out of fear.
5	**B**eat	She is beating the big drum.
6	**B**ounce	She bounced happily and stretched out her right fist.
7	**B**ow	He bowed with both hands, hoping the other would forgive him.
8	**B**rush	She brushed the dust off the table.
9	**C**arry	A worker is carrying a box.
10	**C**ast	The fisherman casts his net into the river.
11	**C**lap	The teacher clapped his hands to signal the students to be quiet.
12	**C**rouch	He crouched down to tie his shoelaces.
...	...	...
9998	**Z**ip	She zipped up his backpack.
9999	**Z**oom	He suddenly paused mid-walk, then zoomed around to turn right and walked off.

(a) Representative text descriptions

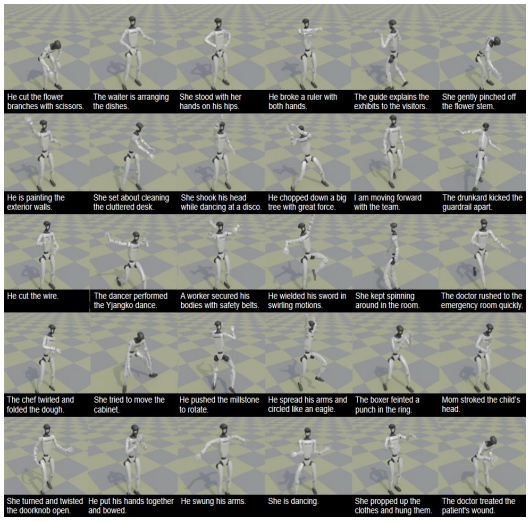

(b) Rendered motion frames

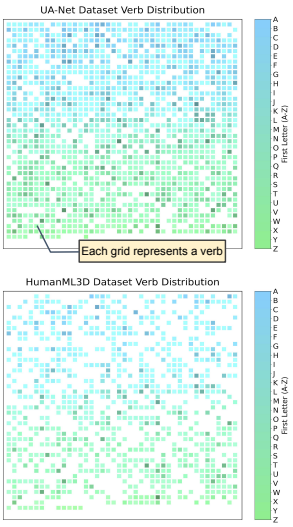

(c) Action verb diversity

Figure 3. **UA-Net dataset analysis.** (a) Representative text descriptions of human motions from UA-Net. (b) Rendered motion frames corresponding to selected descriptions. (c) Action verb diversity comparison: we visualize the presence of 1684 common verbs on a square grid organized alphabetically (A–Z), where each cell represents a verb. UA-Net demonstrates significantly broader vocabulary coverage compared to HumanML3D [18]. (Vector graphics; zoom for details.)

efficiency with low latency, we adopt a chunked decoding strategy where decoding is triggered only when accumulated tokens reach a predefined chunk size, reducing overhead while maintaining responsive motion generation.

3.5. Real-time motion streaming

We implement a server-client streaming architecture that decouples computationally intensive motion generation (server-side) from real-time robot control (client-side). When instructions are provided through the client interface, the commands are forwarded to the GPU-equipped server, which tokenizes the multimodal instruction and feeds it to the Qwen2.5 model for autoregressive motion generation. Generated tokens are continuously decoded and streamed to the client via low-latency WebSocket communication. To ensure smooth transitions between consecutive instructions, we maintain 10 motion tokens as history context when processing new commands.

The server generates motions faster than real-time, creating a temporal mismatch between the server's variable generation rate and the client's fixed 50 Hz control frequency. We address this through a client-side motion cache that accumulates incoming frames from the server. The client queries this buffer at precise 20 ms intervals, ensuring consistent reference motion delivery to the tracking controller regardless of server-side generation speed variations. This decoupling guarantees smooth playback even when the generation experiences momentary slowdowns or speedups.

3.6. Humanoid motion tracking

The decoded motion sequences are streamed to a modified BeyondMimic [36] tracker that serves as the low-level controller. We adapt the original tracker by removing the global orientation component from the reference motion observation, allowing the policy to focus exclusively on relative joint configurations rather than absolute orientation:

$$\mathbf{o}_t = [\mathbf{q}_t^{\text{ref}}, \dot{\mathbf{q}}_t^{\text{ref}}, \mathbf{q}_t^{\text{curr}}, \dot{\mathbf{q}}_t^{\text{curr}}, \mathbf{g}_t, \omega_t, \mathbf{a}_{t-1}], \tag{6}$$

where $\mathbf{q}_t^{\text{ref}}$ represents the decoded reference joint positions, $\mathbf{q}_t^{\text{curr}}$ denotes the current robot joint state, $\mathbf{g}_t$ is the gravity vector in the robot's body frame, ω_t is the angular velocity, and $\mathbf{a}_{t-1}$ is the previous action.

The tracker outputs target joint positions $\mathbf{p}_t$ that drive the robot to follow the generated motion while maintaining dynamic balance and physical feasibility (see Sec. B.2 for training details). By decoupling high-level motion generation from low-level control, this architecture enables robust execution even under external disturbances, as the tracker can reactively adjust joint commands while preserving the overall motion intent.

4. The UA-Net dataset

We present UA-Net, a comprehensive multimodal humanoid motion dataset comprising text-to-motion, trajectory-to-motion, and music-to-motion modalities. UA-Net combines our collected MoCap data for text and trajectory conditioning with the existing FineDance dataset [31] for music. All human motions are retargeted to humanoid-compatible formats using GMR [79], with manual refinement to preserve motion fidelity while respecting humanoid physical constraints (see Sec. D for details).

Table 1. **Multimodal humanoid control evaluation.** We compare UniAct against baselines across text, trajectory, and music modalities. Metrics include FID (motion quality), Diversity (motion variation), MM-dist (text-motion alignment), R-precision (retrieval accuracy at top-1/2/3), Root error (trajectory tracking accuracy in meters), Genre (genre fidelity for dance), and Success rate (task completion without falls). Arrows indicate better direction. We ablate FSQ codebook size (0.25× codes) and downsampling rate (2× downsampled). UniAct achieves superior performance across most metrics while maintaining lower diversity than diffusion-based two-step methods.

Modality	Method	FID ↓	Diversity ↑	MM-dist ↓	R-precision ↑			Root error ↓	Genre ↑	Success rate ↑
					R@1	R@2	R@3			
Text	LangWBC [60]	5.17	5.03	4.19	10.21	14.47	19.73	-	-	58.2
	UH-1 [45]	6.39	5.41	4.45	12.73	14.30	17.23	-	-	51.3
	OmniH2O [20]+MDM [66]	3.11	**5.88**	3.29	18.01	25.42	27.94	-	-	63.0
	BeyondMimic [36]+MDM [66]	2.93	5.72	2.93	24.53	28.78	34.68	-	-	65.3
	Ours	**1.69**	5.21	**2.45**	**41.59**	**54.28**	**60.63**	-	-	**83.1**
	Ours (0.25× codes)	1.84	5.04	2.67	33.19	36.42	38.75	-	-	79.6
	Ours (2× downsamp.)	1.73	4.92	2.51	38.03	50.90	58.13	-	-	80.9
Trajectory	OmniH2O [20]+MDM [66]	2.62	3.42	2.75	11.41	19.06	24.74	1.392	-	23.6
	BeyondMimic [36]+MDM [66]	2.58	**3.53**	2.65	12.33	17.23	27.16	1.284	-	35.2
	Ours	**0.77**	3.01	**1.77**	**56.15**	**65.26**	**71.43**	**0.151**	-	**97.3**
	Ours (0.25× codes)	0.80	3.02	1.78	55.60	60.32	65.89	0.195	-	94.3
	Ours (2× downsamp.)	0.79	3.13	1.82	54.18	63.15	69.90	0.163	-	95.8
Music	OmniH2O [20]+MDM [66]	2.35	4.50	3.59	15.64	21.27	23.43	-	0.84	45.8
	BeyondMimic [36]+MDM [66]	1.97	**4.66**	3.37	17.91	21.20	26.59	-	0.77	57.1
	Ours	**1.53**	4.34	**2.61**	**53.13**	**65.05**	**69.82**	-	**0.97**	**87.4**
	Ours (0.25× codes)	1.74	4.42	2.79	48.10	61.92	66.86	-	0.88	75.6
	Ours (2× downsampled)	1.58	4.31	2.84	45.63	58.99	66.91	-	0.80	84.4

4.1. Dataset modalities

Text-to-motion contains 20 hours of motion paired with natural language descriptions, ranging from simple atomic actions to complex compositional movements (Fig. 3). Each sequence is organized in lexicographic order based on its primary description, creating a structured taxonomy from basic locomotion (*e.g.* 'backward stepping,' 'forward walking') to complex interactions (*e.g.* 'cooking,' 'door opening'). Fig. 3(c) shows that UA-Net provides broader coverage of common verbs compared to HumanML3D [18], critical for robot motion training and evaluation.

Trajectory-to-motion comprises 20 minutes of walking conditioned on spatial trajectories, including point-to-point navigation, curved paths, and obstacle avoidance. Speed variations span from 0.3 m/s to 1.5 m/s, with annotations specifying velocity, curvature, and heading angle at 120 Hz.

Music-to-motion incorporates 376 retargeted dance sequences from FineDance [31], spanning multiple genres and tempos. Retargeting preserves rhythmic synchronization while adapting movements to humanoid kinematic and dynamic constraints.

4.2. MoCap configuration

We employ an OptiTrack MoCap with 48 high-speed cameras operating at 120 Hz in a 10×8×4 meter capture volume. Data collection uses a 43-marker configuration with additional hand and foot markers for fine-grained MoCap. We recruited 10 professional performers, including dancers, athletes, and motion specialists, to ensure diverse styles.

The GMR [79] pipeline maps captured motions to a 29-DoF humanoid model compatible with Unitree G1, incorporating collision avoidance, joint limits, and balance constraints. All sequences undergo manual verification to validate foot contact preservation, center of mass trajectories, and dynamic feasibility.

5. Experiments and results

We conduct comprehensive experiments to validate UniAct across three key dimensions: (i) multimodal humanoid control that surpasses strong baselines, (ii) real-time system performance through detailed timing analysis, (iii) motion tokenizer robustness under disturbances and OOD motions.

5.1. Multimodal humanoid control

We evaluate UniAct's ability to control humanoid robots through diverse input modalities: text, trajectory, and music. From UA-Net, we exclude motion sequences involving sitting on chairs, lying down, or stair climbing to ensure physical feasibility in our evaluation environment. The dataset is partitioned with 80% for training and 20% for evaluation. Each experiment involves providing a single instruction and evaluating the resulting motion quality.

Experimental protocol For text-to-motion, we provide single sentences from the test set as input, allowing the humanoid to execute actions until reaching the end-of-motion token. For trajectory-to-motion, we select 10-second walking trajectory segments from the test set and autoregressively drive the humanoid to follow the specified

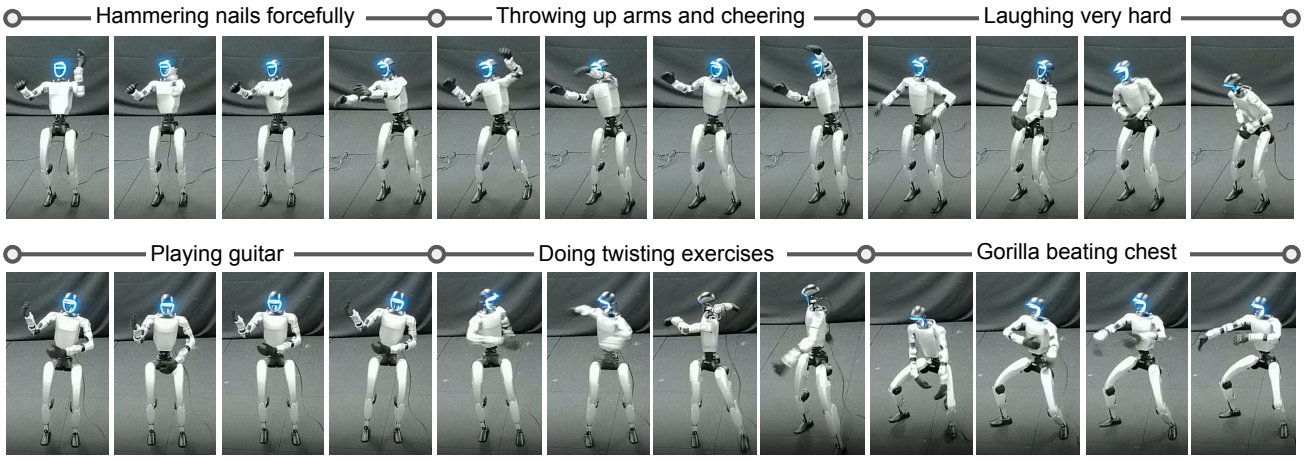

(a) Sequential language-to-motion

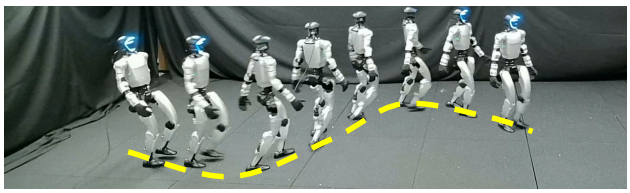

(b) Trajectory-to-motion

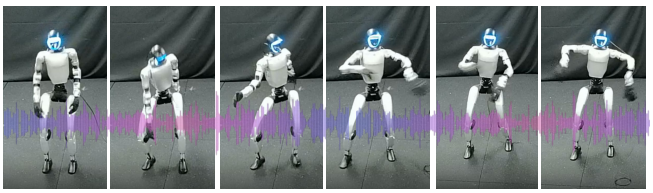

(c) Music-to-motion

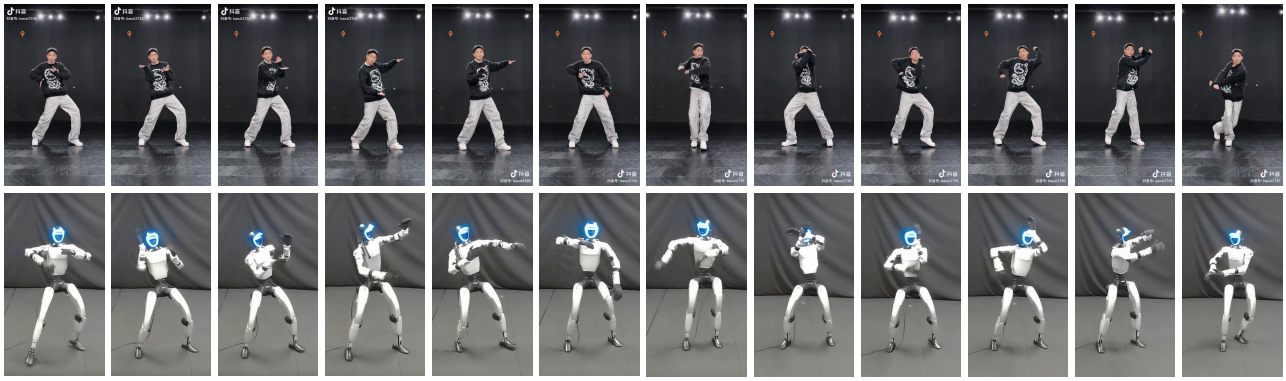

(d) Zero-shot human-to-humanoid motion

Figure 4. **Qualitative results of UniAct across diverse instruction modalities.** (a) Sequential text-to-motion: the humanoid executes a sequence of complex actions following instructions. (b) Trajectory-to-motion: the robot follows a curved path (yellow dashed line) with natural walking motions. (c) Music-to-motion: the humanoid generates dance movements synchronized to the music's rhythm. (d) Zero-shot human-to-humanoid motion transfer: retarget motions from internet videos to humanoid execution without additional training.

path. For music-to-motion, we randomly sample 10-second music clips from FineDance.

Strong baselines and ablations We compare UniAct against several SOTA baselines. LangWBC [60] and UH-1 [45] directly map text instructions to actions. OmniH2O [20] and BeyondMimic [36] combined with MDM-generated [66] motions serve as two-step methods. Baseline adaptation details are in Sec. C.1. Additionally, we ablate: (i) FSQ codebook size, and (ii) FSQ downsampling rates.

Evaluation metrics Following Guo et al. [18], we measure robot motion execution quality in simulation through Fréchet Inception Distance (FID), diversity, multimodal distance (MM-dist), and R-precision. Success rate indicates the percentage of trials where the robot completes tasks without falling or significant instruction deviation. For trajectory-following, we quantify tracking accuracy using root mean square error (RMSE) between generated and target trajectories. For dance generation, we introduce a genre fidelity metric measuring the distance between generated dance motions and each dataset genre. All experiments are conducted in MuJoCo with contact dynamics and actuator models. Metric formulations are in Sec. C.2.

Results As Tab. 1 shows, UniAct achieves the highest performance across most metrics. For text-to-motion, we

Table 2. **Motion tracking evaluation with discrete motion representation.** We evaluate BeyondMimic [36] tracking performance with and without our FSQ-based tokenizer across three settings: low-quality reference motions, unseen OOD motions, and training set reconstruction. Metrics include MPJPE (cm), Error vel. (cm/s), and Success rate. Arrows indicate better direction. Our tokenizer improves robustness on noisy and OOD motions while maintaining reconstruction quality.

Method	Low-quality reference motions			Unseen motion generation			Quantative error analysis		
	MPJPE ↓	Error vel. ↓	Suc. rate ↑	MPJPE ↓	Error vel. ↓	Suc. rate ↑	MPJPE ↓	Error vel. ↓	Suc. rate ↑
BeyondMimic [36]+FSQ (Ours)	**36.10**	**52.62**	**95.4**	**45.61**	**31.60**	**95.2**	14.48	22.06	**100.0**
BeyondMimic [36]+FSQ (0.25× codes)	50.90	61.99	90.5	51.33	37.49	91.0	23.32	25.02	**100.0**
BeyondMimic [36]+FSQ (2× downsampled)	46.19	60.29	88.4	57.78	37.44	87.2	20.07	23.10	**100.0**
BeyondMimic [36]	68.34	66.86	76.2	48.93	37.35	90.5	**12.59**	**19.99**	**100.0**

Table 3. **Computational timing breakdown (ms).** We measure latency components across different hardware configurations. Model latency is the sum of motion generation, token decode, and motion track. Total delay additionally includes data transmission when transitioning to new commands. All methods achieve real-time performance at 20 Hz control frequency.

Hardware	Motion generation	Token decode	Motion track	Data transmission	Model latency	Total delay
H100	14.1	0.98	3.49	33.5	52.1	264
RTX 5090	18.7	1.05	6.59	33.5	59.8	340
RTX 4090	26.2	1.20	7.06	33.5	68.0	461

demonstrate strong text-motion alignment and high success rates, highlighting UniAct's ability to generate accurate and robust motions from instructions. For trajectory-following, UniAct achieves the lowest mean root error, demonstrating superior locomotion capabilities. For music-to-dance, we produce strong genre correspondence, effectively matching dance movements to musical styles. While our diversity scores are lower than two-step methods, this is partly attributed to the inherently high diversity of diffusion-based motion generation, which may produce more varied but potentially less controlled outputs. Fig. 4 shows qualitative results of UniAct across diverse instruction modalities.

5.2. Computational time analysis

Real-time performance is critical for UniAct. We quantify system latency through two metrics: total delay (latency when transitioning to new commands) and model latency (latency during ongoing instruction streaming).

Tab. 3 breaks down timing into four components: (i) motion generation, time from instruction receipt to first motion token; (ii) token decoding, conversion from discrete tokens to continuous DoF positions; (iii) motion tracking, low-level controller computation time; and (iv) data transmission, network latency between server and client.

5.3. Motion tracking evaluation

We validate that discrete motion representation enhances tracking robustness without compromising fidelity. Using BeyondMimic [36], we track motions after encoding, quantizing, and decoding. Performance is measured via MPJPE, joint velocity error, and success rate across three settings:

Low-quality reference motions We add Gaussian noise and temporal jitter to UA-Net motions, simulating imperfect inputs. Comparing tracking performance after discrete processing against original unperturbed references tests whether quantization refines noisy inputs (Sec. E).

Unseen motion generalization We collect 50 online videos beyond UA-Net's training distribution, extract SMPL-X parameters [48] via GVHMR [61], and retarget to G1 DoF via GMR [79]. Comparing performance with/without discrete representation demonstrates how tokenization constrains motions to physically feasible spaces.

Quantization error analysis We evaluate reconstruction error on training motions across different configurations, varying FSQ codebook size and downsampling rate.

Results Tab. 2 shows our tracker maintains higher success rates on reference motions with jitter or OOD characteristics without quality degradation, demonstrating UniAct maps motions into the seen domain for robust control.

5.4. Compositional cross-modal control

UniAct enables cross-modal control by independently generating upper-body actions and lower-body trajectories, then fusing them into coherent whole-body movements. Fine-tuning the tracking policy with composed pairs ensures stable execution. This allows expressive actions (*e.g.*, waving, drumming) while following paths. Zero-shot generalization to unseen action-trajectory combinations enhances behavioral diversity and deployment scalability (Sec. F).

6. Conclusion

We introduce UniAct, a unified framework for real-time multimodal humanoid control with sub-500 ms response latency. By integrating multimodal large language models with efficient motion tokenization, UniAct translates diverse inputs—text, vision, and audio—into robust robot motions through a shared discrete token representation. Extensive real-world experiments demonstrate superior performance across multimodal tasks while maintaining robustness to noisy and OOD inputs. We also establish a comprehensive benchmark and dataset with standardized evaluation protocols for the research community.

Limitation The system struggles with highly dynamic movements (*e.g.*, rapid jumping) due to motion tracker constraints, and currently lacks object manipulation capabilities. Future work could develop more robust controllers for high-speed motions and incorporate object-centric representations to enable contact-rich manipulation tasks.

Acknowledgement This work is supported in part by the National Science and Technology Innovation 2030 Major Program (2025ZD0219400), the National Natural Science Foundation of China (62376009 to Y. Zhu and 6247070125 to Y. Wang), the PKU-BingJi Joint Laboratory for Artificial Intelligence, and the National Comprehensive Experimental Base for Governance of Intelligent Society, Wuhan East Lake High-Tech Development Zone. This project would not have been possible without the yearlong collaboration with Virtual Point, whose partnership has been instrumental to this work. We are deeply grateful to Peiyuan Zhi and Le Ma from BIGAI, and Wenhua Xia and Rui Chen from the PKU-Wuhan Institute of Artificial Intelligence for their invaluable hardware support and technical assistance throughout the development process. We also extend our sincere thanks to Yutang Lin and Yixuan Li for their insightful discussions and feedback that helped shape the ideas presented in this work. Finally, we thank all the team members who contributed to the countless hours of physical robot experiments and debugging that made this system a reality.

References

[1] Hyemin Ahn, Timothy Ha, Yunho Choi, Hwiyeon Yoo, and Songhwai Oh. Text2action: Generative adversarial synthesis from language to action. In *IEEE International Conference on Robotics and Automation (ICRA)*, 2018. 3

[2] Chaitanya Ahuja and Louis-Philippe Morency. Language2pose: Natural language grounded pose forecasting. In *International Conference on 3D Vision (3DV)*, 2019. 3

[3] Simon Alexanderson, Rajmund Nagy, Jonas Beskow, and Gustav Eje Henter. Listen, denoise, action! audio-driven motion synthesis with diffusion models. *ACM Transactions on Graphics (TOG)*, 42(4):1–20, 2023. 3

[4] Shuai Bai, Keqin Chen, Xuejing Liu, Jialin Wang, Wenbin Ge, Sibo Song, Kai Dang, Peng Wang, Shijie Wang, Jun Tang, Humen Zhong, Yuanzhi Zhu, Mingkun Yang, Zhaohai Li, Jianqiang Wan, Pengfei Wang, Wei Ding, Zheren Fu, Yiheng Xu, Jiabo Ye, Xi Zhang, Tianbao Xie, Zesen Cheng, Hang Zhang, Zhibo Yang, Haiyang Xu, and Junyang Lin. Qwen2.5-vl technical report, 2025. 4, A2

[5] Yuxuan Bian, Ailing Zeng, Xuan Ju, Xian Liu, Zhaoyang Zhang, Wei Liu, and Qiang Xu. Motioncraft: Crafting whole-body motion with plug-and-play multimodal controls. In *Proceedings of AAAI Conference on Artificial Intelligence (AAAI)*, 2025. 3

[6] Michael Bloesch, Jan Humplik, Viorica Patraucean, Roland Hafner, Tuomas Haarnoja, Arunkumar Byravan, Noah Yamamoto Siegel, Saran Tunyasuvunakool, Federico Casarini, Nathan Batchelor, et al. Towards real robot learning in the wild: A case study in bipedal locomotion. In *Conference on Robot Learning (CoRL)*, 2021. 2

[7] Anthony Brohan, Noah Brown, Justice Carbajal, Yevgen Chebotar, Joseph Dabis, Chelsea Finn, Keerthana Gopalakrishnan, Karol Hausman, Alex Herzog, Jasmine Hsu, et al. Rt-1: Robotics transformer for real-world control at scale. In *Robotics: Science and Systems (RSS)*, 2023. 3

[8] Rui Chen, Mingyi Shi, Shaoli Huang, Ping Tan, Taku Komura, and Xuelin Chen. Taming diffusion probabilistic models for character control. In *SIGGRAPH Conference Proceedings*, pages 1–10, 2024. 2

[9] Xin Chen, Biao Jiang, Wen Liu, Zilong Huang, Bin Fu, Tao Chen, and Gang Yu. Executing your commands via motion diffusion in latent space. In *Proceedings of Conference on Computer Vision and Pattern Recognition (CVPR)*, 2023. 3

[10] Simon Clavet. Motion matching and the road to next-gen animation. In *Proc. of GDC*, 2016. A3

[11] Jieming Cui, Tengyu Liu, Nian Liu, Yaodong Yang, Yixin Zhu, and Siyuan Huang. Anyskill: Learning open-vocabulary physical skill for interactive agents. In *Proceedings of Conference on Computer Vision and Pattern Recognition (CVPR)*, 2024. 2

[12] Pengxiang Ding, Jianfei Ma, Xinyang Tong, Binghong Zou, Xinxin Luo, Yiguo Fan, Ting Wang, Hongchao Lu, Panzhong Mo, Jinxin Liu, et al. Humanoid-vla: Towards universal humanoid control with visual integration. *arXiv preprint arXiv:2502.14795*, 2025. 3

[13] Danny Driess, Fei Xia, Mehdi SM Sajjadi, Corey Lynch, Aakanksha Chowdhery, Ayzaan Wahid, Jonathan Tompson, Quan Vuong, Tianhe Yu, Wenlong Huang, et al. Palm-e: An embodied multimodal language model. In *Proceedings of International Conference on Machine Learning (ICML)*, 2023. 3

[14] Helei Duan, Jeremy Dao, Kevin Green, Taylor Apgar, Alan Fern, and Jonathan Hurst. Learning task space actions for bipedal locomotion. In *IEEE International Conference on Robotics and Automation (ICRA)*, 2021. 2

[15] Ke Fan, Shunlin Lu, Minyue Dai, Runyi Yu, Lixing Xiao, Zhiyang Dou, Junting Dong, Lizhuang Ma, and Jingbo Wang. Go to zero: Towards zero-shot motion generation with million-scale data. In *Proceedings of International Conference on Computer Vision (ICCV)*, 2025. 3

[16] Xinmin Fang, Lingfeng Tao, and Zhengxiong Li. Ai robotics open source r&d survey: Foundation models, datasets, simulation, and benchmarks platforms (2023-2025). *Authorea Preprints*, 2025. 3

[17] Zipeng Fu, Qingqing Zhao, Qi Wu, Gordon Wetzstein, and Chelsea Finn. Humanplus: Humanoid shadowing and imitation from humans. In *Conference on Robot Learning (CoRL)*, 2024. 2

[18] Chuan Guo, Shihao Zou, Xinxin Zuo, Sen Wang, Wei Ji, Xingyu Li, and Li Cheng. Generating diverse and natural 3d human motions from text. In *Proceedings of Conference on Computer Vision and Pattern Recognition (CVPR)*, 2022. 3, 5, 6, 7, A3, A4

[19] Félix G Harvey, Mike Yurick, Derek Nowrouzezahrai, and Christopher Pal. Robust motion in-betweening. *ACM Transactions on Graphics (TOG)*, 39(4):60–1, 2020. 3

[20] Tairan He, Zhengyi Luo, Xialin He, Wenli Xiao, Chong Zhang, Weinan Zhang, Kris Kitani, Changliu Liu, and Guanya Shi. Omnih2o: Universal and dexterous human-to-humanoid whole-body teleoperation and learning. In *Conference on Robot Learning (CoRL)*, 2024. 2, 3, 6, 7, A2

[21] Tairan He, Zhengyi Luo, Wenli Xiao, Chong Zhang, Kris Kitani, Changliu Liu, and Guanya Shi. Learning human-to-humanoid real-time whole-body teleoperation. In *IEEE/RSJ International Conference on Intelligent Robots and Systems (IROS)*, 2024. 3

[22] Tairan He, Jiawei Gao, Wenli Xiao, Yuanhang Zhang, Zi Wang, Jiashun Wang, Zhengyi Luo, Guanqi He, Nikhil Sobanbab, Chaoyi Pan, et al. Asap: Aligning simulation and real-world physics for learning agile humanoid whole-body skills. In *Robotics: Science and Systems (RSS)*, 2025. 2

[23] Tairan He, Wenli Xiao, Toru Lin, Zhengyi Luo, Zhenjia Xu, Zhenyu Jiang, Jan Kautz, Changliu Liu, Guanya Shi, Xiaolong Wang, et al. Hover: Versatile neural whole-body controller for humanoid robots. In *IEEE International Conference on Robotics and Automation (ICRA)*, 2025. 2

[24] Fangzhou Hong, Mingyuan Zhang, Liang Pan, Zhongang Cai, Lei Yang, and Ziwei Liu. Avatarclip: zero-shot text-driven generation and animation of 3d avatars. *ACM Transactions on Graphics (TOG)*, 41(4), 2022. 3

[25] Mazeyu Ji, Xuanbin Peng, Fangchen Liu, Jialong Li, Ge Yang, Xuxin Cheng, and Xiaolong Wang. Exbody2: Advanced expressive humanoid whole-body control. *arXiv preprint arXiv:2412.13196*, 2024. 2

[26] Korrawe Karunratanakul, Konpat Preechakul, Supasorn Suwajanakorn, and Siyu Tang. Guided motion diffusion for controllable human motion synthesis. In *Proceedings of Conference on Computer Vision and Pattern Recognition (CVPR)*, 2023. 3

[27] Nhat Le, Thang Pham, Tuong Do, Erman Tjiputra, Quang D Tran, and Anh Nguyen. Music-driven group choreography. In *Proceedings of Conference on Computer Vision and Pattern Recognition (CVPR)*, 2023. 3

[28] Jiaman Li, Jiajun Wu, and C Karen Liu. Object motion guided human motion synthesis. *ACM Transactions on Graphics (TOG)*, 42(6):1–11, 2023. 3

[29] Jialong Li, Xuxin Cheng, Tianshu Huang, Shiqi Yang, Ri-Zhao Qiu, and Xiaolong Wang. Amo: Adaptive motion optimization for hyper-dexterous humanoid whole-body control. In *Robotics: Science and Systems (RSS)*, 2025. 2

[30] Ruilong Li, Shan Yang, David A Ross, and Angjoo Kanazawa. Ai choreographer: Music conditioned 3d dance generation with aist++. In *Proceedings of International Conference on Computer Vision (ICCV)*, 2021. 4

[31] Ronghui Li, Junfan Zhao, Yachao Zhang, Mingyang Su, Zeping Ren, Han Zhang, Yansong Tang, and Xiu Li. Finedance: A fine-grained choreography dataset for 3d full body dance generation. In *Proceedings of International Conference on Computer Vision (ICCV)*, 2023. 3, 5, 6

[32] Yixuan Li, Yutang Lin, Jieming Cui, Tengyu Liu, Wei Liang, Yixin Zhu, and Siyuan Huang. Clone: Closed-loop whole-body humanoid teleoperation for long-horizon tasks. In *CoRL*, 2025. 2

[33] Zhe Li, Yisheng He, Lei Zhong, Weichao Shen, Qi Zuo, Lingteng Qiu, Zilong Dong, Laurence Tianruo Yang, and Weihao Yuan. Mulsmo: Multimodal stylized motion generation by bidirectional control flow. *arXiv preprint arXiv:2412.09901*, 2024. 3

[34] Zhe Li, Cheng Chi, Yangyang Wei, Boan Zhu, Yibo Peng, Tao Huang, Pengwei Wang, Zhongyuan Wang, Shanghang Zhang, and Chang Xu. From language to locomotion: Retargeting-free humanoid control via motion latent guidance. *arXiv preprint arXiv:2510.14952*, 2025. 2, 3

[35] Zhe Li, Weihao Yuan, Weichao Shen, Siyu Zhu, Zilong Dong, and Chang Xu. Omnimotion: Multimodal motion generation with continuous masked autoregression. *arXiv preprint arXiv:2510.14954*, 2025. 3

[36] Qiayuan Liao, Takara E Truong, Xiaoyu Huang, Guy Tevet, Koushil Sreenath, and C Karen Liu. Beyondmimic: From motion tracking to versatile humanoid control via guided diffusion. *arXiv preprint arXiv:2508.08241*, 2025. 2, 5, 6, 7, 8, A2, A5

[37] Angela S Lin, Lemeng Wu, Rodolfo Corona, Kevin Tai, Qixing Huang, and Raymond J Mooney. Generating animated videos of human activities from natural language descriptions. In *Proceedings of Advances in Neural Information Processing Systems (NeurIPS)*, 2018. 3

[38] Xiao Lin and Mohamed R Amer. Human motion modeling using dvgans. *arXiv preprint arXiv:1804.10652*, 2018. 3

[39] Junfeng Long, Junli Ren, Moji Shi, Zirui Wang, Tao Huang, Ping Luo, and Jiangmiao Pang. Learning humanoid locomotion with perceptive internal model. In *IEEE International Conference on Robotics and Automation (ICRA)*, 2025. 2

[40] Qiujing Lu, Yipeng Zhang, Mingjian Lu, and Vwani Roychowdhury. Action-conditioned on-demand motion generation. In *Proceedings of the 30th ACM International Conference on Multimedia*, 2022. 3

[41] Shunlin Lu, Ling-Hao Chen, Ailing Zeng, Jing Lin, Ruimao Zhang, Lei Zhang, and Heung-Yeung Shum. Humantomato: Text-aligned whole-body motion generation. In *Proceedings of International Conference on Machine Learning (ICML)*, 2024. 3

[42] Mingshuang Luo, Ruibing Hou, Zhuo Li, Hong Chang, Zimo Liu, Yaowei Wang, and Shiguang Shan. M3gpt: An advanced multimodal, multitask framework for motion comprehension and generation. In *Proceedings of Advances in Neural Information Processing Systems (NeurIPS)*, 2024. 2, 3

[43] Zhengyi Luo, Jinkun Cao, Kris Kitani, Weipeng Xu, et al. Perpetual humanoid control for real-time simulated avatars. In *Proceedings of International Conference on Computer Vision (ICCV)*, pages 10895–10904, 2023. 2, 3

[44] Naureen Mahmood, Nima Ghorbani, Nikolaus F Troje, Gerard Pons-Moll, and Michael J Black. Amass: Archive of motion capture as surface shapes. In *Proceedings of International Conference on Computer Vision (ICCV)*, 2019. 3

[45] Jiageng Mao, Siheng Zhao, Siqi Song, Tianheng Shi, Junjie Ye, Mingtong Zhang, Haoran Geng, Jitendra Malik, Vitor Guizilini, and Yue Wang. Learning from massive human videos for universal humanoid pose control. *arXiv preprint arXiv:2412.14172*, 2024. 2, 6, 7, A2

[46] Fabian Mentzer, David Minnen, Eirikur Agustsson, and Michael Tschannen. Finite scalar quantization: Vq-vae made simple. *arXiv preprint arXiv:2309.15505*, 2023. 3, A1, A5

[47] Liang Pan, Zeshi Yang, Zhiyang Dou, Wenjia Wang, Buzhen Huang, Bo Dai, Taku Komura, and Jingbo Wang. Tokenhsi: Unified synthesis of physical human-scene interactions through task tokenization. In *Proceedings of Conference on Computer Vision and Pattern Recognition (CVPR)*, 2025. 2

[48] Georgios Pavlakos, Vasileios Choutas, Nima Ghorbani, Timo Bolkart, Ahmed A. A. Osman, Dimitrios Tzionas, and Michael J. Black. Expressive body capture: 3D hands, face, and body from a single image. In *Proceedings of Conference on Computer Vision and Pattern Recognition (CVPR)*, 2019. 8, A1, A3

[49] Xue Bin Peng, Pieter Abbeel, Sergey Levine, and Michiel Van de Panne. Deepmimic: Example-guided deep reinforcement learning of physics-based character skills. *ACM Transactions on Graphics (TOG)*, 37(4):1–14, 2018. 2

[50] Xue Bin Peng, Ze Ma, Pieter Abbeel, Sergey Levine, and Angjoo Kanazawa. Amp: Adversarial motion priors for stylized physics-based character control. *ACM Transactions on Graphics (TOG)*, 40(4):1–20, 2021. 2

[51] Xue Bin Peng, Yunrong Guo, Lina Halper, Sergey Levine, and Sanja Fidler. Ase: Large-scale reusable adversarial skill embeddings for physically simulated characters. *ACM Transactions on Graphics (TOG)*, 41(4):1–17, 2022. 2

[52] Mathis Petrovich, Michael J Black, and Gül Varol. Temos: Generating diverse human motions from textual descriptions. In *Proceedings of European Conference on Computer Vision (ECCV)*, 2022. 3

[53] Mathis Petrovich, Michael J Black, and Gül Varol. Tmr: Text-to-motion retrieval using contrastive 3d human motion synthesis. In *Proceedings of International Conference on Computer Vision (ICCV)*, 2023. 3, A3

[54] Ekkasit Pinyoanuntapong, Muhammad Saleem, Korrawe Karunratanakul, Pu Wang, Hongfei Xue, Chen Chen, Chuan Guo, Junli Cao, Jian Ren, and Sergey Tulyakov. Maskcontrol: Spatio-temporal control for masked motion synthesis. In *Proceedings of International Conference on Computer Vision (ICCV)*, 2025. 3

[55] Matthias Plappert, Christian Mandery, and Tamim Asfour. Learning a bidirectional mapping between human whole-body motion and natural language using deep recurrent neural networks. *Robotics and Autonomous Systems*, 109:13–26, 2018. 3

[56] Ilija Radosavovic, Sarthak Kamat, Trevor Darrell, and Jitendra Malik. Learning humanoid locomotion over challenging terrain. *arXiv preprint arXiv:2410.03654*, 2024. 2

[57] Ilija Radosavovic, Tete Xiao, Bike Zhang, Trevor Darrell, Jitendra Malik, and Koushil Sreenath. Real-world humanoid locomotion with reinforcement learning. *Science Robotics*, 9(89):eadi9579, 2024. 2

[58] John Schulman, Filip Wolski, Prafulla Dhariwal, Alec Radford, and Oleg Klimov. Proximal policy optimization algorithms. *arXiv preprint arXiv:1707.06347*, 2017. A2

[59] Agon Serifi, Ruben Grandia, Espen Knoop, Markus Gross, and Moritz Bächer. Vmp: Versatile motion priors for robustly tracking motion on physical characters. In *Computer graphics forum*, 2024. 2

[60] Yiyang Shao, Xiaoyu Huang, Bike Zhang, Qiayuan Liao, Yuman Gao, Yufeng Chi, Zhongyu Li, Sophia Shao, and Koushil Sreenath. Langwbc: Language-directed humanoid whole-body control via end-to-end learning. In *Robotics: Science and Systems (RSS)*, 2025. 2, 3, 6, 7, A2

[61] Zehong Shen, Huaijin Pi, Yan Xia, Zhi Cen, Sida Peng, Zechen Hu, Hujun Bao, Ruizhen Hu, and Xiaowei Zhou. World-grounded human motion recovery via gravity-view coordinates. In *SIGGRAPH Asia Conference Proceedings*, 2024. 8

[62] Jiangxin Sun, Chunyu Wang, Huang Hu, Hanjiang Lai, Zhi Jin, and Jian-Fang Hu. You never stop dancing: Non-freezing dance generation via bank-constrained manifold projection. In *Proceedings of Advances in Neural Information Processing Systems (NeurIPS)*, 2022. 3

[63] Wandong Sun, Baoshi Cao, Long Chen, Yongbo Su, Yang Liu, Zongwu Xie, and Hong Liu. Learning perceptive humanoid locomotion over challenging terrain. *arXiv preprint arXiv:2503.00692*, 2025. 2

[64] Chen Tessler, Yunrong Guo, Ofir Nabati, Gal Chechik, and Xue Bin Peng. Maskedmimic: Unified physics-based character control through masked motion inpainting. *ACM Transactions on Graphics (TOG)*, 43(6):1–21, 2024. 2

[65] Guy Tevet, Brian Gordon, Amir Hertz, Amit H Bermano, and Daniel Cohen-Or. Motionclip: Exposing human motion generation to clip space. In *Proceedings of European Conference on Computer Vision (ECCV)*, 2022. 3

[66] Guy Tevet, Sigal Raab, Brian Gordon, Yonatan Shafir, Daniel Cohen-Or, and Amit H Bermano. Human motion diffusion model. In *Proceedings of International Conference on Learning Representations (ICLR)*, 2022. 3, 6, 7, A3

[67] Guy Tevet, Sigal Raab, Setareh Cohan, Daniele Reda, Zhengyi Luo, Xue Bin Peng, Amit H Bermano, and Michiel van de Panne. Closd: Closing the loop between simulation and diffusion for multi-task character control. In *Proceedings of International Conference on Learning Representations (ICLR)*, 2025. 2

[68] Andrea Tirinzoni, Ahmed Touati, Jesse Farebrother, Mateusz Guzek, Anssi Kanervisto, Yingchen Xu, Alessandro Lazaric, and Matteo Pirotta. Zero-shot whole-body humanoid control via behavioral foundation models. *arXiv preprint arXiv:2504.11054*, 2025. 2

[69] Jonathan Tseng, Rodrigo Castellon, and Karen Liu. Edge: Editable dance generation from music. In *Proceedings of Conference on Computer Vision and Pattern Recognition (CVPR)*, 2023. 3

[70] Guillermo Valle-Pérez, Gustav Eje Henter, Jonas Beskow, Andre Holzapfel, Pierre-Yves Oudeyer, and Simon Alexanderson. Transflower: probabilistic autoregressive dance generation with multimodal attention. *ACM Transactions on Graphics (TOG)*, 40(6):1–14, 2021. 3

[71] Homer Walke, Kevin Black, Abraham Lee, Moo Jin Kim, Max Du, Chongyi Zheng, Tony Zhao, Philippe Hansen-Estruch, Quan Vuong, Andre He, Vivek Myers, Kuan Fang, Chelsea Finn, and Sergey Levine. Bridgedata v2: A dataset for robot learning at scale. In *Conference on Robot Learning (CoRL)*, 2023. 3

[72] Yinhuai Wang, Qihan Zhao, Runyi Yu, Hok Wai Tsui, Ailing Zeng, Jing Lin, Zhengyi Luo, Jiwen Yu, Xiu Li, Qifeng Chen, et al. Skillmimic: Learning basketball interaction skills from demonstrations. In *Proceedings of Conference on Computer Vision and Pattern Recognition (CVPR)*, 2025. 2

[73] Yiming Xie, Varun Jampani, Lei Zhong, Deqing Sun, and Huaizu Jiang. Omnicontrol: Control any joint at any time for human motion generation. In *Proceedings of International Conference on Learning Representations (ICLR)*, 2024. 3

[74] Pei Xu, Xiumin Shang, Victor Zordan, and Ioannis Karamouzas. Composite motion learning with task control. *ACM Transactions on Graphics (TOG)*, 42(4):1–16, 2023. 2

[75] Haoru Xue, Xiaoyu Huang, Dantong Niu, Qiayuan Liao, Thomas Kragerud, Jan Tommy Gravdahl, Xue Bin Peng, Guanya Shi, Trevor Darrell, Koushil Screenath, et al. Leverb: Humanoid whole-body control with latent vision-language instruction. *arXiv preprint arXiv:2506.13751*, 2025. 2, 3

[76] Lujie Yang, Xiaoyu Huang, Zhen Wu, Angjoo Kanazawa, Pieter Abbeel, Carmelo Sferrazza, C Karen Liu, Rocky Duan, and Guanya Shi. Omniretarget: Interaction-preserving data generation for humanoid whole-body loco-manipulation and scene interaction. *arXiv preprint arXiv:2509.26633*, 2025. 3

[77] Kangning Yin, Weishuai Zeng, Ke Fan, Minyue Dai, Zirui Wang, Qiang Zhang, Zheng Tian, Jingbo Wang, Jiangmiao Pang, and Weinan Zhang. Unitracker: Learning universal whole-body motion tracker for humanoid robots. *arXiv preprint arXiv:2507.07356*, 2025. 2

[78] Kevin Zakka. Mink: Python inverse kinematics based on mujoco, july 2024, 2024. GitHub repository. 3

[79] Yanjie Ze, João Pedro Araújo, Jiajun Wu, and C. Karen Liu. Gmr: General motion retargeting, 2025. GitHub repository. 3, 5, 6, 8

[80] Yanjie Ze, Zixuan Chen, JoÃĢo Pedro AraÃšjo, Zi-ang Cao, Xue Bin Peng, Jiajun Wu, and C Karen Liu. Twist: Teleoperated whole-body imitation system. In *Conference on Robot Learning (CoRL)*, 2025. 2, 3

[81] Chong Zhang, Wenli Xiao, Tairan He, and Guanya Shi. Wococo: Learning whole-body humanoid control with sequential contacts. In *Conference on Robot Learning (CoRL)*, 2024. 2

[82] Jianrong Zhang, Yangsong Zhang, Xiaodong Cun, Yong Zhang, Hongwei Zhao, Hongtao Lu, Xi Shen, and Ying Shan. Generating human motion from textual descriptions with discrete representations. In *Proceedings of Conference on Computer Vision and Pattern Recognition (CVPR)*, 2023. 3

[83] Mingyuan Zhang, Zhongang Cai, Liang Pan, Fangzhou Hong, Xinying Guo, Lei Yang, and Ziwei Liu. Motiondiffuse: Text-driven human motion generation with diffusion model. *Transactions on Pattern Analysis and Machine Intelligence (TPAMI)*, 46(6):4115–4128, 2024. 3

[84] Mingyuan Zhang, Daisheng Jin, Chenyang Gu, Fangzhou Hong, Zhongang Cai, Jingfang Huang, Chongzhi Zhang, Xinying Guo, Lei Yang, Ying He, et al. Large motion model for unified multi-modal motion generation. In *Proceedings of European Conference on Computer Vision (ECCV)*, 2024. 2, 3

[85] Peiyuan Zhi, Peiyang Li, Jianqin Yin, Baoxiong Jia, and Siyuan Huang. Learning unified force and position control for legged loco-manipulation. In *Conference on Robot Learning (CoRL)*, 2025. 2

[86] Zixiang Zhou and Baoyuan Wang. Ude: A unified driving engine for human motion generation. In *Proceedings of Conference on Computer Vision and Pattern Recognition (CVPR)*, 2023. 2, 3

A. Additional qualitative results

We present extensive qualitative results of real-world experiments across different modalities: language-to-motion (Fig. A3), music-to-motion (Fig. A4), trajectory-to-motion (Fig. A5), and human-to-humanoid motion (Fig. A6). Additionally, we show examples of cross-modal control in Fig. A7. These results demonstrate that UniAct possesses diverse instruction following capabilities and exhibits robustness in real-world task execution. We highly recommend readers to view our *project website* for a richer visualization of UniAct's performance across diverse scenarios.

B. Implementation details

B.1. Tokenization

Network design The model employs a convolutional autoencoder architecture with Finite Scalar Quantization (FSQ) [46] for discrete latent representation learning. The encoder-decoder framework processes sequences of shape (B, N, D) where B is batch size, N is sequence length, and D is feature dimension.

The encoder consists of an input projection layer followed by two conv blocks with increasing channel capacity. Each conv block contains a strided 1D convolution with kernel size 7 and a residual block. The residual blocks combine 1D convolutions with GroupNorm and per-position MLPs that apply LayerNorm and GELU activations. The encoder reduces the sequence length by a factor of 2 (from N to N/2) while projecting to a 5-dimensional latent space.

The decoder mirrors the encoder architecture with transposed 1D convolutions for upsampling. It takes the quantized latents and upsamples them through upsampling blocks, doubling the temporal resolution while reducing channel dimensions. The final projection layer reconstructs the original input dimension. The model uses hidden dimensions of 256 channels in intermediate layers, with expansion factors in the residual blocks for increased representational capacity. All convolution operations use appropriate padding to maintain temporal alignment throughout the network.

In ablation studies described in Sec. 5, we evaluated two architectural modifications to understand the importance of codebook capacity and temporal resolution. As shown in Tabs. 1 and 2, reducing the codebook size to 0.25× by decreasing quantization levels resulted in performance degradation, indicating that sufficient discrete representation capacity is crucial for capturing the data distribution. Similarly, increasing the downsampling rate to 4 also decreased performance, demonstrating that maintaining adequate temporal resolution in the latent space is essential for accurate reconstruction. Excessive temporal resolution increases computational latency during motion generation. To balance motion quality with real-time performance, we adopt a downsampling rate of 2.

Codebook usage FSQ adapts its codebook size to match the complexity of different modalities. For robot motion, the FSQ quantizer discretizes the continuous degrees of freedom using predefined quantization levels [8, 8, 8, 6, 5] across 5 latent dimensions, yielding a codebook of 8×8×8×6×5=15,360 discrete codes. This larger codebook captures the nuanced variations in joint configurations and dynamic movements required for expressive robot control. In contrast, music representations utilize 6,144 codes to encode audio features, while trajectory data requires only 60 codes due to its lower-dimensional complexity and smoother spatial characteristics.

Our approach directly learns robot motion in the robot's native kinematic space, eliminating the need for post-processing retargeting steps. This end-to-end learning strategy contrasts with conventional pipelines that first generate human motion using human models (such as SMPL-X [48]), then apply optimization-based retargeting to map the motion onto humanoid robots' workspace. Such two-stage approaches introduce cumulative errors from body proportion mismatches, joint limit violations, and the fundamental differences between human and robot morphology. Our quantitative results demonstrate that direct robot motion embedding achieves superior tracking accuracy and naturalness compared to retargeting-based methods, while also reducing computational overhead by avoiding the intermediate human representation and complex optimization procedures required for motion transfer.

The unified codebook is partitioned to accommodate multiple modalities while preserving the original text vocabulary. As listed in Tab. A1, we allocate non-overlapping index ranges for each modality: indices 0–130,076 are reserved for the original text tokens, ensuring compatibility with pretrained language models. Indices 130,077–130,078 correspond to the special tokens <SOM> (start of motion) and <EOM> (end of motion). Subsequently, indices 130,079–145,438 are designated for robot motion codes, 145,439–151,582 represent music tokens, and indices 151,583–151,642 encode trajectory representations. This design enables seamless multi-modal generation within a single autoregressive framework.

Table A1. **Codebook allocation across modalities.**

Modality	Index Range	Codebook Size
Text	0 – 130,076	130,077
<SOM> and <EOM>	130,077 – 130,078	2
Robot Motion	130,079 – 145,438	15,360
Music	145,439 – 151,582	6,144
Trajectory	151,583 – 151,642	60

B.2. Motion tracking

We implement our motion tracking pipeline using PPO [58] to train policies on the Unitree G1 humanoid robot. The framework processes hours-long reference motions from the UA-Net dataset using a unified set of hyperparameters across all motions.

We adapt the motion tracking policy from BeyondMimic by removing global orientation from the reference motion observation, allowing the policy to focus on relative joint configurations:

$$\mathbf{o}_t = [\mathbf{q}_t^{\text{ref}}, \dot{\mathbf{q}}_t^{\text{ref}}, \mathbf{q}_t^{\text{curr}}, \dot{\mathbf{q}}_t^{\text{curr}}, \mathbf{g}_t, \omega_t, \mathbf{a}_{t-1}], \tag{A1}$$

where $\mathbf{q}_t^{\text{ref}}$ and $\dot{\mathbf{q}}_t^{\text{ref}}$ are the decoded reference position and velocity, $\mathbf{q}_t^{\text{curr}}$ and $\dot{\mathbf{q}}_t^{\text{curr}}$ are the current robot joint states, $\mathbf{g}_t$ represents the gravity vector in the robot frame, ω_t represents the angular velocity, and $\mathbf{a}_{t-1}$ represents the robot action at previous timestep. We use asymmetric actor-critic training where the critic additionally receives per-body relative poses for direct Cartesian error estimation.

The tracker outputs joint target positions $\mathbf{p}_t$ that drive the robot to follow the generated motion while maintaining balance and physical feasibility. These are converted to torques through PD control:

$$\boldsymbol{\tau}_j = k_{p,j}(\mathbf{p}_{t,j} - \mathbf{q}_{t,j}^{\text{curr}}) - k_{d,j}\dot{\mathbf{q}}_{t,j}^{\text{curr}}, \tag{A2}$$

where $\boldsymbol{\tau}_j$ is the derived torque applied to each robot joint.

Joint stiffness and damping follow:

$$k_{p,j} = I_j\omega_n^2, \quad k_{d,j} = 2I_j\zeta\omega_n, \tag{A3}$$

with natural frequency $\omega_n = 10$ Hz, overdamped ratio $\zeta = 2$, and reflected inertia $I_j = k_{g,j}^2 I_{\text{motor},j}$.

Reward design The reward function primarily consists of tracking rewards that measure motion accuracy and penalty terms for physical constraints. The tracking rewards include matching the root orientation, body link positions and orientations relative to the root frame, and linear/angular velocities of all tracked links to ensure accurate motion reproduction. Key penalties include action rate regularization to reduce jitter, joint limit violations to prevent hardware damage, and undesired contacts to avoid collisions between non-end-effector body parts and the environment. For more details, please refer to Tab. A3.

Domain randomization We randomize ground friction $\mu \sim \mathcal{U}(0.5, 1.5)$, joint offsets $\Delta q_j \sim \mathcal{U}(-0.05, 0.05)$ rad, and center of mass position $\Delta\mathbf{p}_{\text{CoM}} \sim \mathcal{U}(-0.02, 0.02)$ m.

Training configuration Networks use MLPs with [2048, 1024, 512, 256, 128] hidden units and ELU activations. PPO training uses clip range 0.2, learning rate 1×10^{-3}, discount $\gamma = 0.99$, GAE $\lambda = 0.95$, with 16,384 environments and control frequency 200 Hz (decimation=4).

Table A2. **Reward components and weights for OmniH2O [20].**

Term	Expression	Weight
Penalty		
DoF position limits	$\mathbb{1}(d_t \notin [q_{\min}, q_{\max}])$	-1500
Termination	$\mathbb{1}_{\text{termination}}$	-250
Regularization		
Lower-body action rate	$\|a_t^{\text{lower}} - a_{t-1}^{\text{lower}}\|_2^2$	-2
Upper-body action rate	$\|a_t^{\text{upper}} - a_{t-1}^{\text{upper}}\|_2^2$	-4
Torque	$\|\tau_t\|$	-0.0005
Slippage	$\|v_t^{\text{feet}}\|_2^2 \times \mathbb{1}(F_{\text{feet}} \geqslant 1)$	-5
Task Reward		
DoF position	$\exp(-0.25\|d_t - \tilde{d}_t\|_2)$	100
DoF velocity	$\exp(-0.25\|\dot{d}_t - \tilde{\dot{d}}_t\|_2^2)$	20
Body position	$\exp(-0.5\|p_t - \tilde{p}_t\|_2^2)$	50
Body rotation	$\exp(-0.1\|\theta_t \ominus \tilde{\theta}_t\|)$	50
Body velocity	$\exp(-10.0\|v_t - \tilde{v}_t\|_2)$	20
Body angular velocity	$\exp(-0.01\|\omega_t - \tilde{\omega}_t\|_2)$	20

Table A3. **Reward components and weights for BeyondMimic [36].**

Term	Expression	Weight
Penalty		
Action rate	$\|a_t - a_{t-1}\|_2^2$	-0.1
Joint limit	$\sum_j \mathbb{1}[q_{t,j} \notin [q_{t,j}^{\min}, q_{t,j}^{\max}]]$	-10.0
Undesired contacts	$\sum_{c \notin \{\text{ankles, wrists}\}} \mathbb{1}[\|F_c\| > 1.0\text{N}]$	-0.1
Task Reward		
Root orientation	$\exp\left(-\|o_{t,r}^p - o_{t,r}^g\|_2^2 / 0.4^2\right)$	0.5
Body link pos (rel.)	$\exp\left(-\frac{1}{\|\mathcal{B}\|}\sum_{b\in\mathcal{B}} \|p_{t,b}^{p,\text{rel}} - p_{t,b}^{g,\text{rel}}\|_2^2 / 0.3^2\right)$	1.0
Body link ori (rel.)	$\exp\left(-\frac{1}{\|\mathcal{B}\|}\sum_{b\in\mathcal{B}} \|o_{t,b}^{p,\text{rel}} - o_{t,b}^{g,\text{rel}}\|_2^2 / 0.4^2\right)$	1.0
Body link lin. vel	$\exp\left(-\frac{1}{\|\mathcal{B}\|}\sum_{b\in\mathcal{B}} \|v_{t,b}^p - v_{t,b}^g\|_2^2 / 1.0^2\right)$	1.0
Body link ang. vel	$\exp\left(-\frac{1}{\|\mathcal{B}\|}\sum_{b\in\mathcal{B}} \|\omega_{t,b}^p - \omega_{t,b}^g\|_2^2 / 3.14^2\right)$	1.0

Deployment Policies are exported as PyTorch (.pt) files and deployed at 50 Hz. Each inference step takes about 7ms on an RTX 4090 GPU.

C. Experimental details

C.1. Baseline methods

We apply OmniH2O [20], UH-1 [45], and LangWBC [60] as our baselines. For OmniH2O, we adapt the original settings from the H1 robot to G1, with the adapted parameters shown in Tab. A2. We leverage Qwen2.5-3B [4] throughout these comparisons.

For UH-1, we adopt the end-to-end configuration where the method directly generates robotic actions A_{robot} from text input for open-loop control (text-to-action). To ensure fair comparison with our approach, we train the control policy using the same architecture and training procedure as the motion tracker in UniAct. Specifically, the policy network

learns to map text embeddings directly to joint-level control commands without intermediate motion representation. The parameters are adapted from the original Unitree H1-2 configuration to accommodate the G1 robot.

For LangWBC, we reimplement the method using the BeyondMimic tracker as the teacher policy with reward formulation in Tab. A3. We maintain the original CVAE architecture and DAgger training but scale to 4,096 parallel environments. Unlike the original implementation that tracks only root displacement, we extend the loss computation to whole-body tracking across all keypoints, enabling more accurate motion reproduction on the G1 robot.

We employ the motion diffusion model (MDM) [66] as the motion generator for two-stage baseline methods. The MDM model was trained using motions from the UA-Net training set, which were converted to SMPL-X format [48] for compatibility.

C.2. Evaluation metrics

We leverage multiple metrics to measure UniAct's performance systematically. Following Guo et al. [18] and Tevet et al. [66], we employ FID, Diversity, MM-Dist, and R-precision. FID assesses motion quality by measuring the distance between the distribution of generated motions and training motion data. Diversity measures the generation diversity by calculating the distance between different motion features. MM-Dist and R-precision evaluate the alignment between generated motions and their corresponding multimodal instructions. For text-to-motion, we compute MM-Dist and R-precision using text features corresponding to each motion. For trajectory-to-motion and music-to-motion, we use ground truth motion features to represent instruction features. Following TMR [53], we train motion and text encoders using contrastive learning on the UA-Net dataset to extract motion and text features.

RMSE measures the distance between the robot motion's root and the trajectory in the trajectory-to-motion task. We propose the genre metric to measure the diversity of dance motions generated from music of the same style in the music-to-motion task. It calculates the distance between motion features generated from music of the same genre. Success rate measures the percentage of trials where the robot completes the task without falling or significant deviation from instructions. For text-to-motion, a trial is considered successful if the robot does not fall and the MPJPE between the robot motion and ground truth motion is below 0.8m. For trajectory-to-motion, a trial is considered successful if the robot does not fall and the RMSE is below 1.0m. For music-to-motion, a trial is considered successful if the robot does not fall.

D. The UA-Net dataset

D.1. Trajectory expansion with motion-matching

We collected approximately 20 minutes of human walking motion data on flat terrain using the OptiTrack MoCap system. To obtain paired data of arbitrary trajectories and walking motions, we augmented this dataset using motion matching [10], expanding the walking motion data from 20 minutes in the UA-Net dataset to over 10 hours. This motion-matching-based augmentation pipeline preserves natural locomotion characteristics while following diverse, non-repetitive trajectories. The motion matching pipeline is present in Fig. A2.

Feature extraction In motion matching, each frame is represented by a comprehensive feature vector containing root position and orientation, relative joint positions for lower-body joints (foot and ankles), root and foot velocities, future trajectory points sampled at 20, 40, and 60 frames ahead, and gait phase information derived from foot contact patterns. These features capture both the instantaneous pose and the movement intention, enabling accurate matching between motion clips.

Segmentation process The original 20-minute sequences are segmented into overlapping clips of 2-4 seconds, with cut points determined by gait cycle boundaries at heel-strike events and steady-state walking phases where acceleration is minimal. Each segment maintains at least two complete gait cycles and is annotated with metadata, including walking speed and turning angle. The overlapping strategy ensures multiple transition possibilities from each clip.

Matching and synthesis During synthesis, the system searches for optimal transitions when approaching the last 10 frames of the current clip. The matching cost function evaluates feature similarity through weighted Euclidean distance, velocity consistency, trajectory alignment, and foot contact states. To ensure diversity, we implement a history buffer that penalizes recently used clips and probabilistically select from the top-5 candidates rather than always choosing the best match.

Transitions are blended over 10 frames using spherical linear interpolation for rotations and cubic interpolation for positions. Post-processing applies inverse kinematics to maintain foot contacts during stance phases and smooths trajectories to eliminate artifacts. The pipeline continuously monitors quality metrics, including foot sliding and acceleration discontinuities, automatically filtering problematic sequences.

This approach successfully synthesizes over 10 hours of varied, natural walking motions from the original 20-minute MoCap data, providing sufficient diversity for training trajectory following.

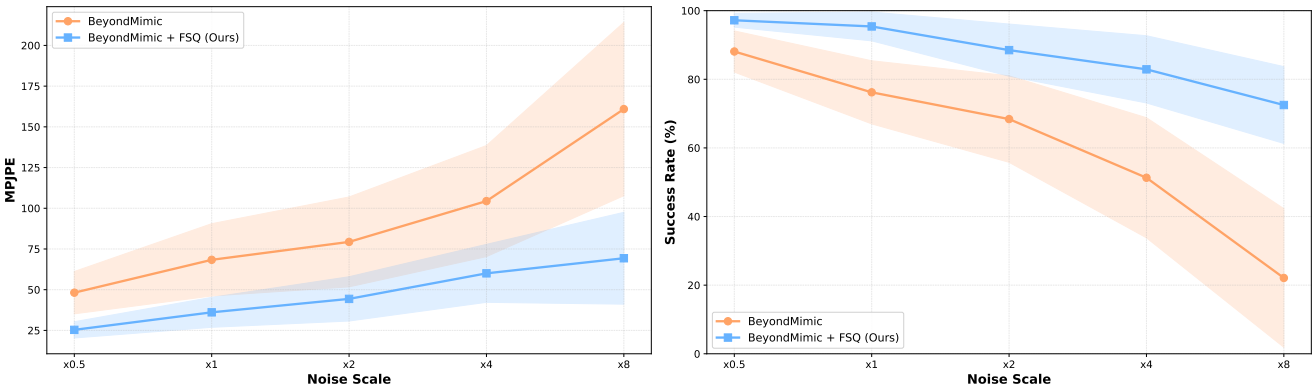

Figure A1. **Performance comparison between BeyondMimic and BeyondMimic + FSQ (ours) under different noise scales.** (left) MPJPE comparison. (right) Success rate comparison. As the noise scale progressively increases, BeyondMimic exhibits significant performance degradation, whereas BeyondMimic + FSQ (ours) maintains relatively low MPJPE and high success rates even at the maximum noise scale (×8), which demonstrates that our quantization approach effectively constrains motions to feasible spaces, enhancing robustness.

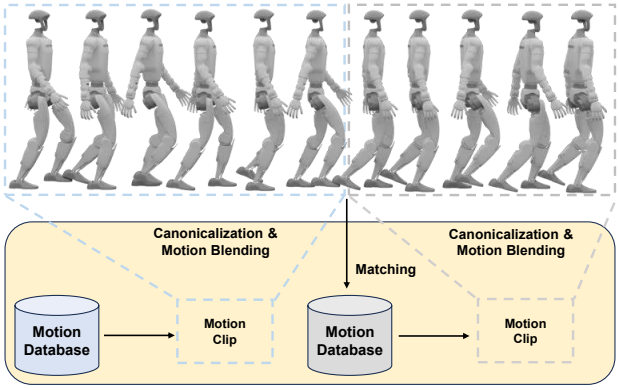

Figure A2. **Overview of motion-matching-based walking motion expansion**. To expand the human walking trajectories in the UA-Net dataset from 20 minutes to over 10 hours, we employ a motion-matching-based augmentation approach. The original motion sequences are segmented into short clips, with each frame represented by features capturing pose, velocity, and future trajectory information. During synthesis, the system continuously searches for optimal clip transitions based on feature similarity and blends them smoothly.

D.2. Text-to-motion from MoCap

The UA-Net dataset comprises over 10,000 expressive motion sequences with meticulously curated motion descriptions. We systematically cover 1,400 common action verbs, representing 1.8× the vocabulary coverage of HumanML3D [18] dataset. For each verb, we compose contextually appropriate sentences that naturally incorporate the verb as the primary action descriptor. High-frequency verbs receive additional instances to reflect their prevalence in real-world applications, with frequently used actions like 'walk,' 'run,' and 'turn' appearing in multiple distinct motion descriptions to ensure comprehensive coverage of common movements.

We employed 10 professional MoCap actors (4 male, 6 female), carefully selected for similar body proportions to minimize morphological variation in the dataset. All actors possess foundational dance training, ensuring they can execute movements with proper body control and spatial awareness. During capture sessions, actors were instructed to perform motions with slight expressiveness beyond everyday movements, adding subtle stylistic flourishes and dynamic variations that enhance the dataset's richness while maintaining naturalness. This directive encouraged actors to interpret each motion with personality rather than mechanical execution, resulting in more engaging and diverse performances that better reflect how humans naturally move when given verbal instructions.

E. Robustness analysis under input corruption

To evaluate whether our discrete representation can effectively refine noisy inputs, we introduce Gaussian noise and temporal jitter to UA-Net motions to simulate low-quality input data. The noise model mimics low-quality MoCap data by incorporating three primary components that represent common tracking artifacts. Given an input motion sequence $\mathbf{X} \in \mathbb{R}^{N \times D}$ with N frames and $D = 29$ degrees of freedom, we generate the noisy output as:

$$\tilde{\mathbf{X}} = \mathbf{X} + \mathbf{n}_{\text{base}} + \mathbf{n}_{\text{burst}} + \mathbf{n}_{\text{jitter}}, \tag{A4}$$

where $\mathbf{n}_{\text{base}} \sim \mathcal{N}(0, \sigma^2_{\text{base}}\mathbf{I})$ with $\sigma_{\text{base}} = 0.01$ represents baseline sensor noise inherent in all MoCap systems. The burst noise $\mathbf{n}_{\text{burst}}$ simulates temporary tracking failures that occur with probability $p_{\text{burst}} = 0.05$ per frame, affecting random subsets of dimensions with temporally correlated Gaussian perturbations $\mathcal{N}(0, \sigma^2_{\text{burst}}\mathbf{I})$ where $\sigma_{\text{burst}} = 0.1$ over durations of 8-20 frames. The jitter noise $\mathbf{n}_{\text{jitter}}$ models sudden tracking spikes that occur with probability $p_{\text{jitter}} = 0.001$ per dimension per frame, introducing large-magnitude disturbances drawn from $\mathcal{N}(0, \sigma^2_{\text{jitter}}\mathbf{I})$ where $\sigma_{\text{jitter}} = 0.3$. Af-

ter processing these corrupted motions through our discrete representation, we compare the tracking performance against the original unperturbed references to assess the quantization's denoising capabilities.

As shown in Tab. 2, all quantization settings achieve significantly better tracking performance compared to the baseline tracking method, where corrupted motions are directly fed into the BeyondMimic motion tracker. This demonstrates that the discrete token representation effectively filters out noise by constraining motions to a finite, well-explored space of learned motion patterns. The quantization process inherently rejects out-of-distribution perturbations and projects noisy inputs onto the manifold of plausible human motions, thereby significantly enhancing tracking robustness even under substantial input corruption.

To further validate the advantages of token-based motion representation, we evaluated the performance of both BeyondMimic [36] and BeyondMimic + FSQ [46] (ours) under varying noise scales. As shown in Fig. A1, as the noise scale progressively increases, BeyondMimic exhibits significant performance degradation, whereas BeyondMimic + FSQ (ours) maintains relatively low MPJPE and high success rates even at the maximum noise scale (×8). This demonstrates that our method can effectively restore the quality of out-of-distribution low-quality data to a certain extent, thereby providing more feasible reference motions for the motion tracking policy.

F. Compositional cross-modal control

UniAct extends naturally to cross-modal humanoid control tasks, where robots must simultaneously process and execute instructions from multiple input modalities. This capability is exemplified by scenarios requiring the robot to perform expressive gestures, such as waving, while simultaneously following a specified trajectory. Such multi-modal control is crucial for practical deployment scenarios where robots must navigate through environments while maintaining meaningful interactions with humans.

Our approach leverages a key observation: expressive semantic actions predominantly manifest in the upper body of humanoid robots, while trajectory following primarily engages lower-body locomotion. Given this observation, we independently generate motions from language and trajectory instructions, then synthesize composed motion by combining the upper-body motion from text-conditioned generation with the lower-body motion from trajectory-conditioned generation. Each robot joint belongs to either the upper body or the lower body, with the pelvis joint serving as the boundary. The pelvis joint itself belongs to the lower body to maintain stable locomotion dynamics. The composed motion is subsequently forwarded to the motion tracking policy for real-world execution.

To ensure robust tracking of these compositionally generated motions, we implement a fine-tuning strategy for the tracking policy. During fine-tuning, we systematically compose motions by randomly pairing lower-body segments from trajectory data with upper-body segments from other motion categories within the UA-Net dataset. This augmentation strategy exposes the tracking policy to motion patterns structurally similar to those encountered during cross-modal inference, enabling the successful execution of previously unseen cross-modal compositions. Fig. A7 illustrates the results from our cross-modal experiments, demonstrating coherent execution of combined instructions.

This compositional approach enables zero-shot generalization to novel motion-trajectory combinations. For instance, despite the training dataset containing only stationary versions of actions such as 'making a phone call' or 'playing drums', our method successfully controls the robot to perform these actions while following arbitrary trajectories. This capability significantly expands the robot's behavioral diversity without requiring exhaustive data collection for every possible combination of actions and trajectories, thereby demonstrating the scalability and practical utility of our framework for real-world humanoid deployment.

Figure A3. **Qualitative results of language-conditioned humanoid control**.

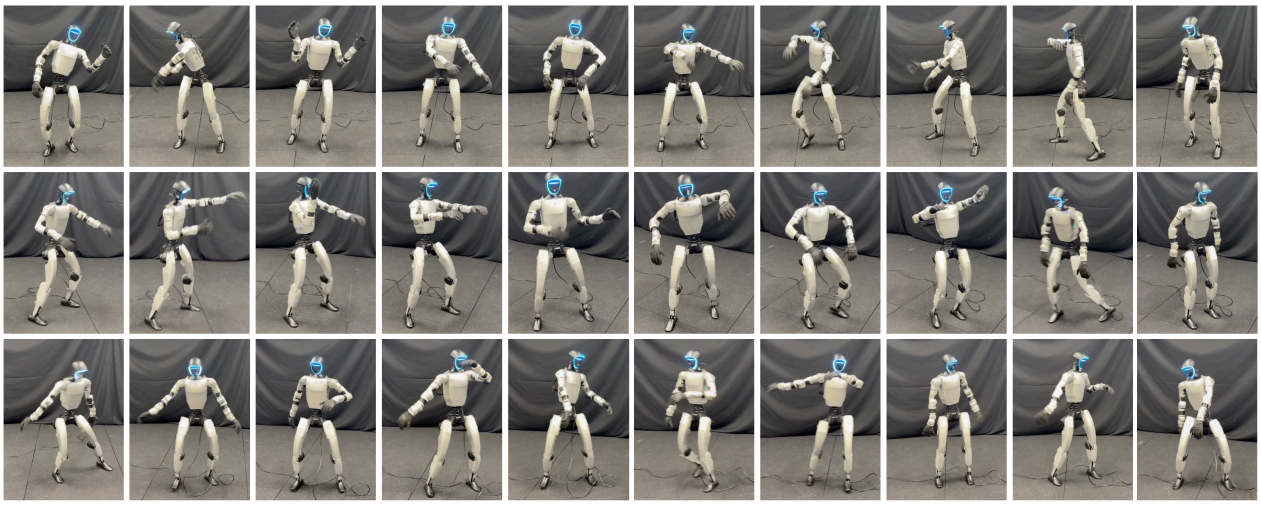

Figure A4. **Qualitative results of music-conditioned humanoid control**.

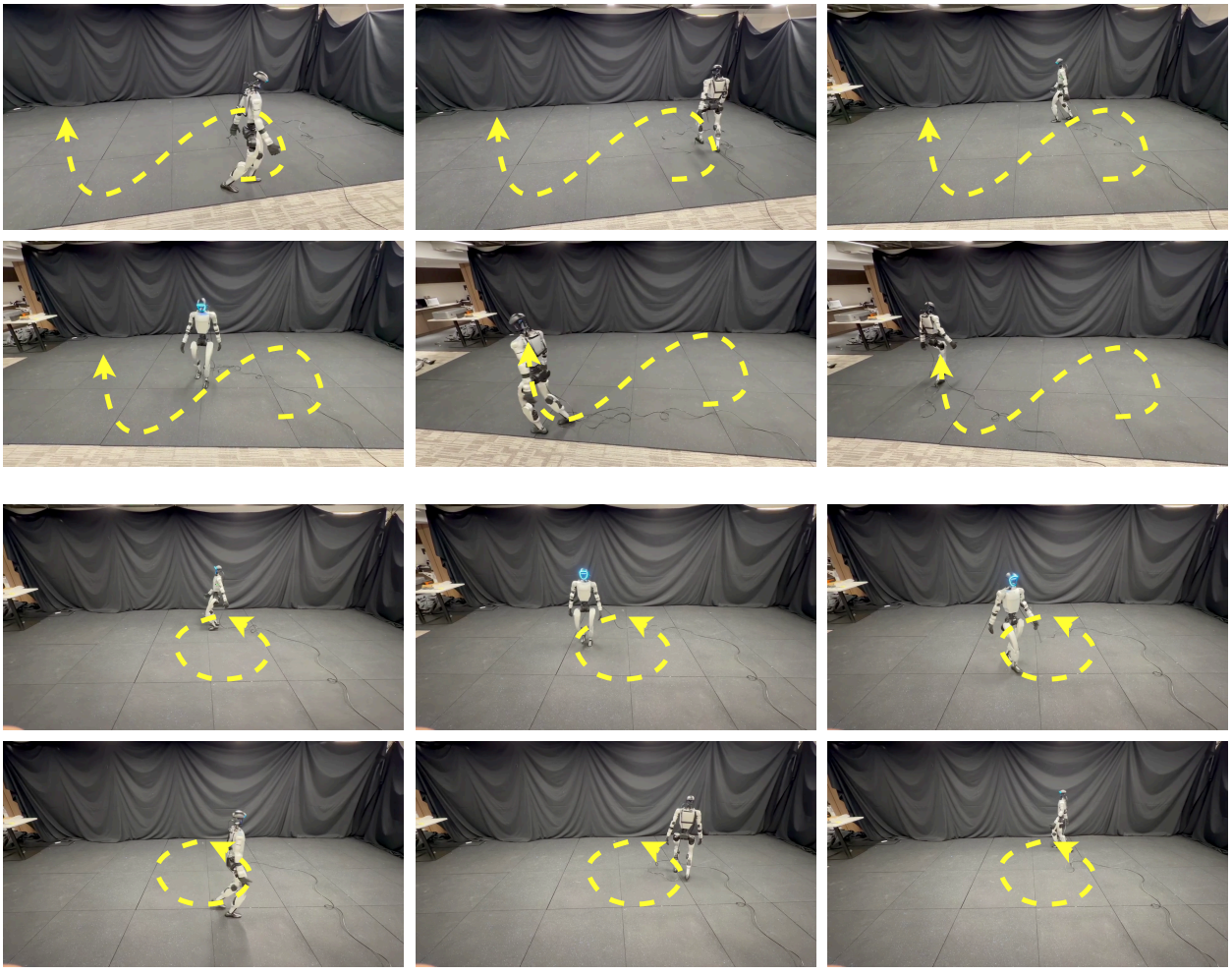

Figure A5. **Qualitative results of trajectory-conditioned humanoid control**.

Figure A6. **Qualitative results of human-to-humanoid motion control**.

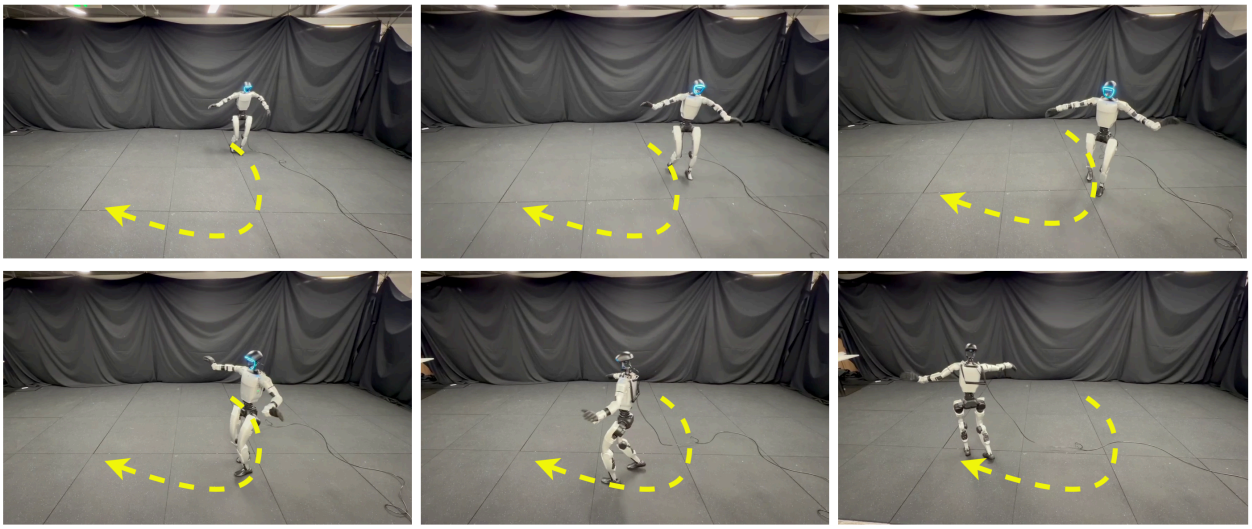

He spreads his arms and twists like a jellyfish.

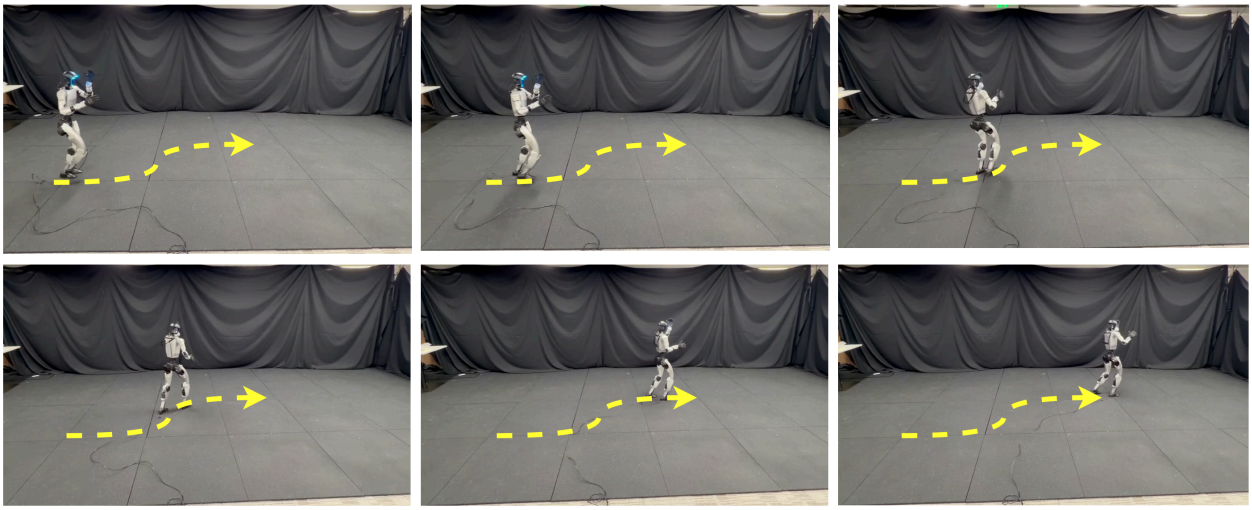

She is talking on the phone.

Figure A7. **Qualitative results of cross-modal humanoid control**.